Colloid and Polymer Science
https://doi.org/10.1007/s00396-018-4401-0

ORIGINAL CONTRIBUTION

The adsorption property and mechanism of phenyl/amine end-capped tetraaniline for alizarin red S

Yunpeng Liu[1] · Jingjing Li[2] · Jinwei Zhu[1,3] · Wei Lyu[1] · Hao Xu[1] · Jiangtao Feng[1] · Wei Yan[1]

Received: 17 January 2018 / Revised: 19 August 2018 / Accepted: 30 August 2018

Abstract

Phenyl/amine end-capped tetraaniline (TANI) was synthesized by chemical polymerization using ferric perchloride ($FeCl_3$) as the oxidant in HCl aqueous solution. And the TANI in emeraldine base state (TANI-EB) was obtained by dedoping the as-prepared TANI in the mixture solution of ammonium hydroxide and acetone. BET surface area (S_{BET}) and zeta potential analysis were used for the adsorption characterization of TANI-EB. The as-prepared TANI-EB was employed as the model compound of PANI to study the adsorption performance of the aniline polymers for organic dye (Alizarin Red S, ARS). In the adsorption study, the effects of pH, doses of adsorbent, and temperature on adsorption kinetics were investigated. The impact of salt ion ($NaNO_3$) concentration on the adsorption performance were also explored. Langmuir isotherm was found to be the most appropriate to describe ARS removal from water by TANI-EB adsorption. The adsorption capacity can be up to 236 mg/g and the equilibrium can reach within 30 min. Thermodynamic parameters, such as delta enthalpy (ΔH), entropy (ΔS), and free energy (ΔG), were also evaluated. Finally, the electrostatic effect and π-π interaction between ARS and the as-prepared TANI-EB in the adsorption process were investigated by UV-Vis spectrum and Fourier transform-infrared spectrum (FT-IR). It illustrates that the adsorption behavior of dye on PANI can be better understood by using TANI as the model compound of PANI. And TANI in EB phase can be as an adsorbent to remove dye from aqueous solution.

Keywords Tetraaniline (TANI) · Alizarin red S (ARS) · Adsorption · Electrostatic interaction · π-π interaction

Introduction

Adsorption technique is regarded as the most efficient and economic method to removal the contaminants from wastewater for its low cost, easy to implement, abundant raw materials, and consuming low energy [1]. Furthermore, the adsorption process can work at room temperature without any hazardous byproducts [2, 3]. These advantages make adsorption a superior way for the pollutant removal from the environment [4, 5] . Indeed, several adsorbents have been employed to remove contaminants from environment [6]. Although the activated carbon is an effective and widely applied adsorbent, the high regeneration cost and low adsorption capacity are the main reasons for its limited application. Therefore, more and more interests in finding and designing cheaper and more effective materials as the potential adsorbent have been stimulated. Various type materials were prepared to adsorb contaminants, such as metal-organic frameworks [7], graphene [8], metal oxide [9], complex substances [10, 11], and conducting polymers [12, 13].

Polyaniline (PANI) is a conducting polymer that has been widely studied for its stability, ease of synthesis, tunable properties, and economic feasibility [14]. As a conducting polymer, PANI has a simple and reversible doping/dedoping performance enabling to control its physicochemical properties, such as conductivity, solubility, and morphology [14, 15]. Therefore, PANI can be widely used in sensors [16], super-capacitors [17], and energy storage [18]. Recently, PANI was also employed

Electronic supplementary material The online version of this article (https://doi.org/10.1007/s00396-018-4401-0) contains supplementary material, which is available to authorized users.

✉ Jiangtao Feng
fjtes@xjtu.edu.cn

[1] Department of Environmental Science and Engineering, Xi'an Jiaotong University, Xi'an 710049, People's Republic of China

[2] Materials Genome Institute of Shanghai University, Shanghai University, Shanghai 200444, People's Republic of China

[3] Shaanxi Electrical Equipment Institution, Xi'an 710025, People's Republic of China

Published online: 08 September 2018

to remove organic and inorganic contaminants from aqueous solution with rapid adsorption for its reversible doping/dedoping performance. For instance, PANI nanoparticles were synthesized by chemical oxidation and it exhibited a rapid adsorption performance for methylene blue (MB) within 60 min [19]. The hollow and core-shell PANI micro/nanospheres had excellent adsorption capacity for methyl orange up to 384.62 mg/g in 30 min [20]. Furthermore, *p*-toluenesulfonic acid (PTSA) and camphorsulfonic acid (CSA)-doped PANI brought out higher adsorption capacity for anionic dyes (such as Orange-G and Alizarine cyanine Green) than that doped with inorganic acid (HCl). And the possible chemical interactions between the negatively charged sulfonated groups of the dyes and the positively charged sites in PANI backbone were considered as the main mechanism in the adsorption process [21, 22]. Meanwhile, the composites of PANI with other materials could further improve their adsorption properties. Zhou et al. confirmed that the Fe_3O_4@PANI core-shell materials showed great adsorption performance for bisphenol A (BPA), α-naphthol and β-naphthol from water solution. The composites exhibited strong affinity to the organic chemicals containing benzene ring because of π-π interactions and electrostatic interaction [23]. And PANI can be grafted onto the graphene oxide (GO) nanosheets forming PANI@GO composite, which can effectively remove radionuclides U(VI), Eu(III), Sr(II), and Cs(I) from aqueous solutions with the chemical interaction between nitrogen-containing functional groups and the radionuclides [24]. However, PANI is a mixture with different long-chain structures [25], which results in the difficulty to study the specific adsorption mechanism of PANI and adsorbates.

Oligo(aniline)s are a class of conjugated oligomeric materials that can act as model compounds of the PANI [26, 27]. These conjugated oligomeric materials have attracted increasing interests because they not only retain the unique optical and electrical properties of PANI, but also possess excellent well-defined molecular structures [28, 29]. Among the oligo(aniline)s, phenyl/amine end-capped tetraaniline (TANI), the shortest oligomer representing the emeraldine oxidation state, is an important model compound for polyaniline [26].

Herein, phenyl/amine end-capped tetraaniline (Ph/NH_2 TANI) in emeraldine base (EB, both the oxidative and chemical doping routes of Ph/NH_2 TANI is showed in Fig. S1) state was employed to study the adsorption mechanism of the polymers for the anionic dye. And alizarin red S (ARS) was as the target removed compound. The adsorption kinetics, isothermal and thermodynamic, were detailedly studied. And the interaction between the TANI and ARS was also studied. This study would give insight into the adsorption mechanism of polyaniline and organic contaminants.

Experimental section

Materials

N-Phenyl-1, 4-phenylenediamine ($C_{12}H_{12}N_2$, 184.24 g/mol, 98%) was purchased from Aldrich Chemical Co. Ltd. Alizarin Red S ($C_{14}H_7NaO_7S$, 342.26 g/mol, 98%, the molecular structure is shown in Fig. 1, and the UV-Vis absorbance curves, including the photograph in different pH value, of ARS solution were shown in Fig. S2 and Fig. S3) was obtained from Sinopharm Chemical Reagent Co. Ltd.(China), and other chemicals were also from Sinopharm Chemical Reagent Co. Ltd., China. All chemicals were used as received.

Synthesis of Ph/NH_2 TANI-EB

The synthesis method of Ph/NH_2 TANI in emeraldine base state (TANI-EB) referred to the literature [30]. In a typical process, ferric chloride hexahydrate (2.70 g, 10.0 mmol) was dissolved into HCl solution (10 ml, 0.1 M), which was labeled as solution A. The hydrochloride salt of N-phenyl-1, 4-phenylenediamine (dianiline salt, 2.56 g, 10 mmol) was suspended into HCl solution (50 ml, 0.1 M), named as solution B. Solution A was quickly poured into solution B with vigorously mechanical agitation. After stirring for 2 h, the product was collected by centrifugation and washed repeatedly with 0.1 M HCl until the supernatant became colorless. The collected solid was purified by Soxhlet extraction with acetone for 12 h to remove other impurities. The resulting solid was dedoped with a mixture of ammonium hydroxide solution (2 M, 50 ml) and acetone (300 ml) for 30 min. After that, the acetone was removed under the reduced pressure. The precipitate was collected by centrifugation and dried in a vacuum oven at 50 °C for 48 h. The final solid was labeled as TANI-EB and used as the adsorbent in the follow experiments. Characterization of TANI-EB is shown in the ESI, Fig. S4, S5 and Table S1.

Characterizations

BET surface area (S_{BET}), total pore volume (V), and average pore radius (R) were measured at 77 K on Builder SSA-4200 (Beijing, China). UV-Vis spectra were obtained in an Agilent

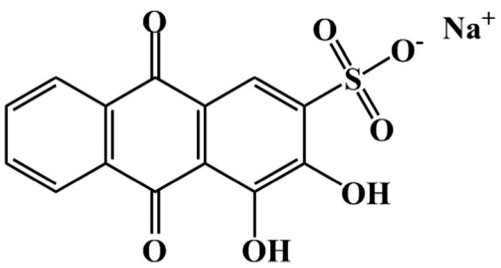

Fig. 1 The molecular structure of ARS

8453 spectrophotometer. Zeta potential of the sample was tested with Malvern Zetasizer Nano ZS90. The sample for zeta potential measurement was prepared by adding 5 mg of TANI-EB into 10 mL NaCl solution (10^{-3} mol/L) at different pH values from 2 to 12 (adjusted with 0.1 mol/L HNO_3 or NaOH solution). Fourier transform infrared spectra (FT-IR) were carried out on BRUKER TENSOR 37 FT-IR spectrophotometer in the range of 4000–400 cm^{-1} by the KBr pellet method. Powder X-ray diffraction (XRD) patterns of the TANI-EB sample was taken on a Rigaku Dmax-RA with a scanning rate of 4 degree/min. Scanning electron microscopy(SEM) images were performed on a JEOL JSM-6390A Field Emission Scanning Electron Microscope with an energy-dispersive spectrometer (EDS).^{1}H NMR experiments was performed using a 400 MHz Varian VNMR 400 NMR spectrometer with CD_3CN-d^3 as the solvent. High-resolution mass spectrometry was performed using MicrOTOF II (ESI-TOF) mass spectrometer.

Adsorption experiments

The adsorption of ARS onto the TANI-EB was carried out by shaking the mixture of ARS solution with the as-prepared TANI-EB at 25 °C. Then, the suspension was centrifuged at 4000 rpm for 6 min. The supernatant was analyzed by the UV-Vis spectrophotometer and the absorbance value was read at the wavelength of 336 nm to evaluate the adsorption capacity of ARS onto TANI.

The amount of ARS molecules adsorbed onto the as-prepared TANI-EB Q_t (mg/g) at certain time t was calculated by Eq. (1):

$$Q_t = \frac{C_0 - C_t}{M} \times V \tag{1}$$

where C_0 (mg/L) is the initial concentration of ARS solution; C_t (mg/L) is the residual concentration of the ARS solution at time t (min); V (L) is the solution volume; and M (g) is TANI-EB mass.

The adsorption equilibrium of ARS (200, 300 and 500 mg/L) was carried out at 25°C. Adsorption isotherms of ARS were obtained by mixing 20 mL different concentrations (100–500 mg/L) of ARS solution with 0.04 g of TANI-EB, and then the mixed liquor was being shaken for 120 min in dark. The Langmuir and Freundlich isotherm models, which were often applied to fit the plots of the isotherm experimental data, were described according to Eqs. (2) and (3), respectively:

$$Q_t = \frac{Q\max K_L C_t}{1 + K_L C_t} \tag{2}$$

$$Q_t = K_F C_t^{1/n} \tag{3}$$

where Q_{max} (mg/g) is the maximum monolayer molecular adsorption capacity onto the adsorbent in Langmuir isotherm model; K_L (L/mg) and K_F ($mg^{1-n} \cdot L^n/g$) are the constant of Langmuir and Freundlich isotherm model, respectively. *1/n* represents the degree of adsorption dependence on the equilibrium concentration in Freundlich isotherm model.

In addition, the dimensionless separation factor R_L, an essential characteristic of the Langmuir model to reflect the favorability of an adsorption process, is expressed as:

$$R_L = \frac{1}{1 + K_L C_m} \tag{4}$$

where C_m (mg/L) is the maximum initial concentration of ARS in solution.

In the regeneration study, 300 mg/L ARS solution was being contacted with TANI-EB for 2 h. Then, 0.1 mol/L NaOH was employed as the regeneration agent to release ARS from the exhausted TANI-EB for 20 min. The regenerated TANI-EB was again used as the adsorbent to remove ARS from aqueous solution. And the adsorption capacity of the regenerated TANI-EB was recorded to evaluate the regeneration property of the as-prepared TANI-EB.

Results and discussion

Characterizations of TANI-EB

The BET surface area (S_{BET}), pore volume (V_p) and pore diameter parameters are shown in Table 1.The S_{BET} and pore diameter were calculated from the corresponding nitrogen adsorption-desorption isotherms and the desorption branch of the nitrogen isotherms by the BJH (Barrett-Joyner-Halenda) method, respectively(Fig. S6). It can be seen from the data that the S_{BET} of the as-prepared TANI-EB was small. It can be explained by the fact that the S_{BET} of the TANI-EB greatly depends on the size of the aggregated TANI-EB nanoparticles. The sharp decline in desorption curve for the TANI-EB is indicative of mesoporosity, probably owing to the heterogeneous pore size. The pore radius of the TANI-EB calculated by the BJH method was 7.4 nm, which indicates that the as-prepared TANI-EB has mesoporous structure. Such a structure is resulted from the pores which are formed between TANI-EB particles [31].

The zeta potential change trend of the as-prepared TANI-EB varying with the pH increase is shown in Fig. 2. The isoelectric point (pH_{pzc}) is the pH value when the zeta potential value is zero. The pH_{pzc} value of TANI-EB is approximately 6.8. The zeta potential of the TANI-EB exhibited positive value at lower pH value (pH < 6.8). It can be deduced that

Table 1 Textural properties of the as-prepared TANI-EB

S_{BET} (m^2/g)	V_p (cm^3/g)	r (nm)
3.159	0.011	7.4

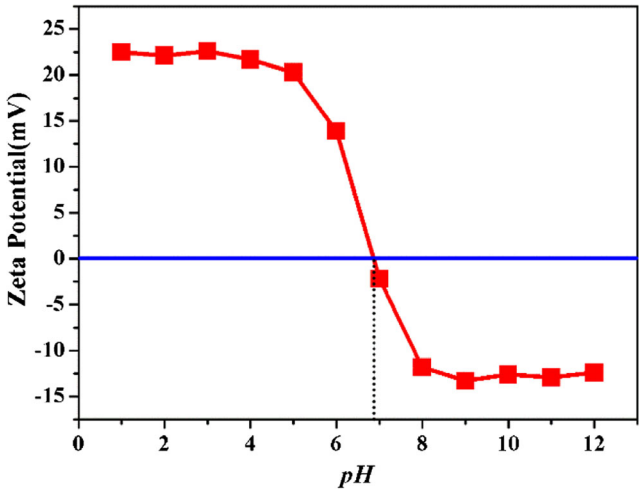

Fig. 2 Zeta potentials of TANI-EB in different pH values

the TANI-EB surface positively charged at lower pH value. The TANI-EB are gradually negatively charged when the pH increased over 6.8. Moreover, the zeta potential at different pH values would affect the interaction between the adsorbent and the adsorbates [32].

Influence factors for adsorption

The effects of several important factors (the initial solution pH, the adsorbent dosage, temperature, the contact time) on ARS adsorbed onto TANI-EB were selected to examine the adsorption performance of the as-prepared TANI-EB.

Effect of the initial solution pH

The initial solution pH is one of the most important factors for the adsorption. The pH variation will result in the characteristic changes on both the adsorbent and the adsorbates and further impact the interaction between them [33]. In this study, the initial solution pH gives a very distinct effect on ARS removal (Fig. 3a). The adsorption capacity is higher in low pH value than that in high pH value, which indicates that electrostatic interaction between the adsorbent and the adsorbates plays an important role in ARS adsorption onto TANI-EB.

Effect of adsorbent dosage

The applied amount of the adsorbent is another important role affecting the adsorption efficiency. Generally, the higher adsorbent dosage will give a better removal efficiency for the increasing quantity of adsorption sites in the high amount of the adsorbent [34]. In this study, different amounts of TANI-EB in the range of 1.0–4.0 g/L were applied to research the effect of the adsorbent dosage. The optimum pH (5–6) value and ARS concentration (300 mg/L) were used. Figure 3b

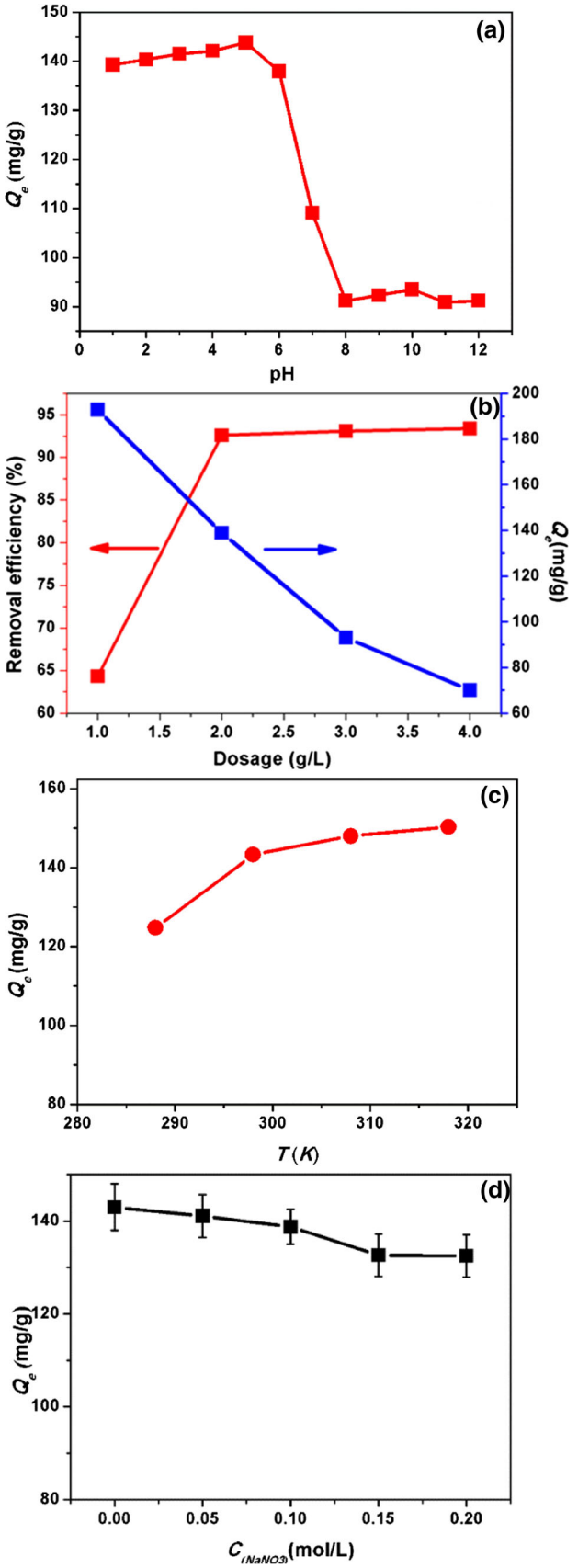

Fig. 3 Effect of pH (**a**), dosage (**b**), temperature (**c**), and ion concentration (**d**) on the ARS adsorbed onto TANI-EB

shows the relationship between the dosage and the ARS removal efficiency. It can be seen that the better removal efficiency was obtained with the increasing dosage, and the removal efficiency does not increase obviously after the dosage is over 2 g/L. The effect of adsorbent dosage gives an idea for the removal of dyes from an economical point of view [35]. Herein, the optimum dosage of TANI-EB for ARS removal was determined as 2.0 g/L in the research condition.

Effect of temperature

The effect of temperature on the adsorption can be employed for explaining adsorption thermodynamics [34]. The adsorption is an endothermic process if the adsorption capacity increases with temperature increasing, which may be due to the enhanced mobility of the adsorbates and an increasing active site on the surface of the adsorbents with the increasing temperature. However, an exothermic adsorption process will also exhibit if the adsorption capacity decrease with the temperature increasing, which may be due to the decrease of the interactions between the adsorbent and the adsorbates at the high temperature [35]. With this aim, the adsorption processes were conducted in the temperature range of 288–318 K (15–45 °C). The adsorption capacity versus temperature is presented in Fig. 3c. The increasing temperature leads to remarkable enhanced adsorption capacity, which demonstrates the endothermic adsorption of the ARS onto TANI-EB.

Effect of the ion concentration

The industrial effluents contain different ions in addition to the dyes, and the ions may compete with the dyes during the adsorption process. The effect of the presence of NO_3^- and Na^+ at different concentrations and the optimum pH under 25 °C on the ARS adsorption onto TANI-EB was also studied (shown in Fig. 3d). The effect of the ionic concentration on the adsorption of ARS onto TANI-EB is unobvious. This result is consistent with Bai's report [36]. In their study, they confirmed that the high ion concentration would reduce the electrostatic repulsion between the adsorbates, which was beneficial to the adsorption. Meanwhile, the high ion concentration could also weaken the electrostatic attraction between adsorbent and adsorbates, which made the adsorption performance decrease. Under these two different functions, the adsorption capacity of ARS onto TANI-EB was almost no change at different ionic concentrations.

The adsorption kinetics and isotherm

The initial ARS concentrations in the range of 200, 300, and 500 mg/L were employed to study the adsorption kinetics of ARS onto the as-prepared TANI-EB. The relative curves for the adsorption time versus the adsorption capacity of TANI-EB for ARS at different initial concentration are shown in the Fig. 4a. As expected, the adsorption capacity increases with the time increasing and finally reaches a plateau, which indicates the dynamic equilibrium exists between the adsorption and desorption, and no more adsorptive molecules would be adsorbed even if the contact time is prolonged. The equilibrium time is also prolonged with the increase of the initial ARS concentration. But the adsorption equilibrium can be reached within 20 min in all the used concentrations.

The adsorption isotherm plays an important role in understanding the mechanism of adsorption. It is significant for giving an idea of adsorption capacity, and can explain the interaction between adsorbent and adsorbates. The surface phase of the adsorbate on the adsorbent may be considered as a monolayer or multilayer [37]. Herein, two important isotherms, Langmuir and Freundlich adsorption models, were used to fit the experimental data. The adsorption isotherm at 25 °C was investigated. The corresponding experimental data fitted Langmuir and Freundlich models are shown in Fig. 4b, and the corresponding parameters are listed in Table 2. It can

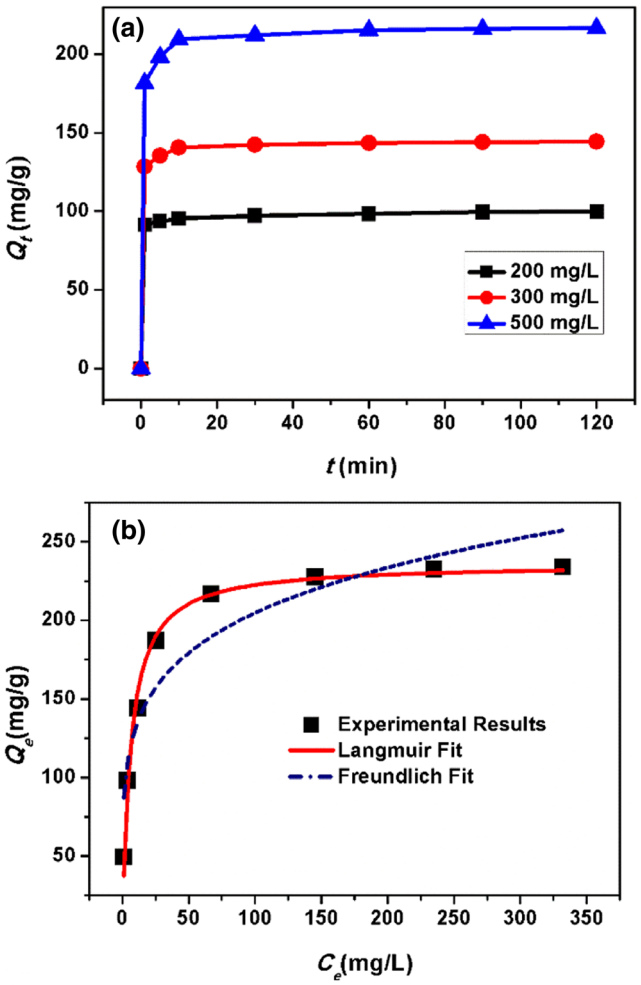

Fig. 4 Plots of Q_t versus time (**a**), Langmuir and Freundlich adsorption isotherms (**b**) for the ARS adsorbed onto TANI-EB

Table 2 Parameters of Langmuir and Freundlich adsorption isotherm models

Langmuir model parameters				Freundlich model parameters		
Q_{max} (mg/g)	K_L(L/mg)	R_L	R^2	K_F (mg^{1-n}·L^n/g)	1/n	R^2
236.09	0.1635	0.0076	0.9894	84.92	0.1910	0.8646

be seen that the correlation coefficient (R^2) for Langmuir model is closed to 1, indicating that Langmuir model is more favorable to describe the adsorption process of ARS onto the as-prepared TANI-EB than that of Freundlich model. It indicates that the adsorption sites on the surface of TANI-EB are uniform and the adsorption of ARS onto the surface of TANI-EB is monolayer. Moreover, the value of R_L is 0.0076 (in the range of 0–1.0), and the value of *1/n* is 0.1910, suggesting that the adsorption of ARS onto the TANI-EB surface is favorable.

Thermodynamic studies

Thermodynamic studies were also performed to explain the adsorption mechanism of ARS molecules onto TANI-EB in detail. The changes of enthalpy (ΔH) and entropy (ΔS) were calculated by the Van't Hoff equation:

$$\ln K_d = -\frac{\Delta H}{RT} + \frac{\Delta S}{R} \tag{5}$$

$$K_d = \frac{Q_e}{C_e} \tag{6}$$

where K_d is the equilibrium constant, R is the gas constant (8.314 J/(K·mol)), and T is the Kelvin temperature. Q_e is the amount of ARS adsorbed onto TANI-EB at equilibrium (mg/g), and C_e is the ARS concentration in the aqueous solution at equilibrium (mg/L), ΔH and ΔS can be calculated from the slope and intercept of the plots of $\ln K_d$ versus $1/T$ (Fig. 5).

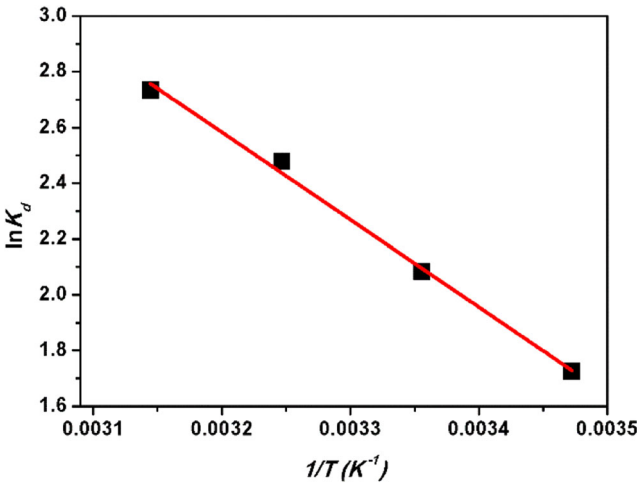

Fig. 5 Plot of $\ln K_d$ vs $1/T$ for the adsorption of ARS onto TANI-EB

The values of Gibb's free energy (ΔG) at different temperatures can be calculated by Eq. 7.

$$\Delta G = -RT \ln K_d \tag{7}$$

The ΔH value was found to be 26.101 kJ/mol, indicating that the adsorption is an endothermic process which is consistent with the result of the temperature effect experiment. The adsorption process is considered as a physical process when the ΔH value is within the range of 1~93 kJ/mol [38]. Whereas the ΔS has a positive value, which reveals the increasing randomness during the adsorption process [39]. All of the ΔG values are negative, indicating the adsorption process is spontaneous (Table 3).

In general, it is typical physisorption when ΔG values are in the range of − 20 ~ 0 kJ/mol, while the ΔG values for chemisorption are in the range of − 400~− 80 kJ/mol [40, 41]. In this study, the values of ΔG are in the range of − 4.126~− 7.228 kJ/mol, which suggests that the adsorption process is physisorption. Meanwhile, the ΔG value decreases with temperature increasing, suggesting that the adsorption is favorable at higher temperature.

Regeneration performance of TANI-EB

In order to study the regeneration performance of TANI-EB, NaOH (0.1 mol/L) and HNO_3 (0.1 mol/L) were employed as the desorption agent and the activate agent respectively for the fact that the adsorption capacity of ARS onto TANI-EB is strongly pH dependent. The activated TANI-EB (2 g/L) was reused to adsorb ARS (300 mg/L) at room temperature, and the results of the adsorption capacity change versus the recycle times were presented in Fig. 6. It can be seen that there is little loss of the adsorption capacity of TANI-EB for ARS after four adsorption-desorption cycles. It is illustrated that the interactions between TANI-EB and ARS can be destroyed by dilute

Table 3 Thermodynamic parameters for the adsorption of ARS onto TANI-EB

T(K)	ΔG(kJ/mol)	ΔH(kJ/mol)	ΔS(J/(mol·K))
288	− 4.128	26.101	105.00
298	− 5.162		
308	− 6.345		
318	− 7.228		

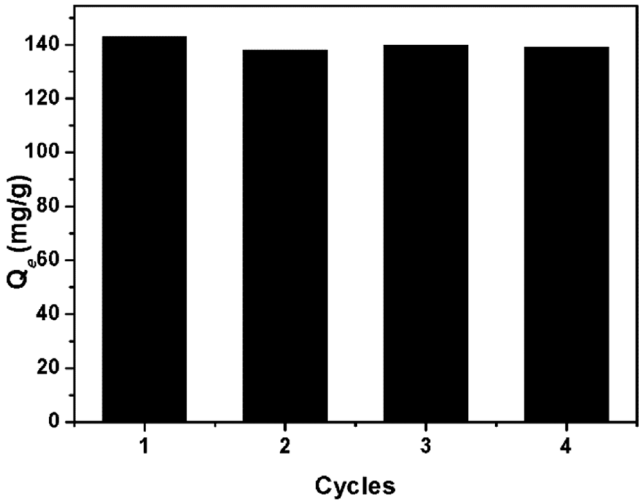

Fig. 6 The adsorption stability of TANI-EB for ARS

NaOH solution and the adsorption performance of TANI-EB can be easily regenerated.

Plausible mechanism of adsorption

The SEM images of the as-prepared TANI-EB and TANI adsorbed ARS are shown in Fig. 7 and EDX images are in Fig. S7 (the important peaks of UV-Vis absorbance for different samples and their assignments shown in Table S2). It can be seen from the SEM images, that the morphology of as-prepared TANI-EB is particles. But the TANI adsorbed ARS exhibits some good crystal structure. While the EDX image of TANI adsorbed ARS displays more sulfur element which is from ARS than that of as-prepared TANI-EB. These phenomena also illustrate that ARS is adsorbed onto the TANI-EB.

The UV-Vis spectra of the samples are presented in Fig. 8. In the UV-Vis spectrum of TANI-EB, two peaks at 317 and 590 nm correspond to the π-π^* transition of benzenoid ring and the benzenoid to quinoid (π_B-π_Q) excitonic transition in TANI-EB [42, 43]. The TANI-desorption sample exhibits the similar UV-Vis spectrum as that of the pristine TANI-EB, indicating the uniform molecular structure before and after adsorption-desorption procedures, which prefigures the reuse of the TANI as an adsorbent without the loss of the adsorption performance. The three characteristic peaks of ARS at 262, 336, and 421 nm are attributed to the n-π^* transition of anthracene, carbonyl, and quinonyl chromophores in anthraquinone dye, respectively [44, 45]. The TANI-adsorption exhibits four peaks. Two of them are the same as TANI-EB at 317, 590 nm (a broad band centered at 590 nm). The peak at 421 and a broad peak centered at 771 nm arise from the polaron-π^* and π-polaron band transitions of TANI in the doping state, respectively [26, 46]. The UV-Vis spectrum of TANI-adsorption indicates that the TANI after adsorbed is only partially doped by the adsorbate for the electrostatic between the positively charged nitrogen atoms in the TANI and the negatively charged -SO_3^- in ARS because of the peaks near 590 and 771 co-exist in the UV-Vis spectrum [47], indicating not all the TANI-EB molecules take part in the adsorption process. Meanwhile, the mixture of ARS and TANI-EB in DMSO solution does not exhibit any apparent absorbance of doping state TANI. This phenomenon confirms that the TANI-EB cannot adsorb (be doped by) ARS in DMSO solution although they can be both dissolved in this solvent and the solution was stirred for 24 h.

The main interaction between ARS and TANI might be the doping effect because TANI-EB can be easily doped by the acidic material in aqueous solution as the pH value of ARS solution is in the range of 4–6 according to the concentration. Moreover, ARS may anchor to the surface of TANI partly by π-π interactions for the π-electron-rich molecular structures of them, which is consistent with the reports that the benzene derivatives can interact through π-π electron donor-accepter interaction with the materials on the π-electron-rich surface [48, 49].

The XRD spectra of the TANI-EB and the TANI adsorbed ARS are presented in Fig. 9 (and the important peaks of XRD patterns for different samples and their assignments was shown in Table S3). The pristine TANI-EB is amorphous. However, TANI-adsorbed ARS exhibits good crystallinity. Three dominant peaks (19.66°, 20.59°, and 25.38°) in the diffraction pattern are the Brogg diffraction peaks for the doped TANI [18]. According to Wang's report, the peaks at 19.66° and 20.59° are for the dopant anion incorporated

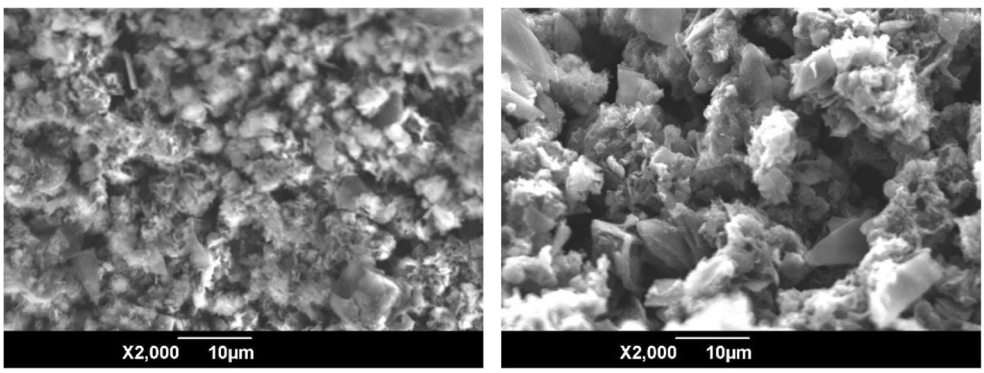

Fig. 7 SEM images of TANI-EB before (**a**) and after (**b**) adsorbed ARS

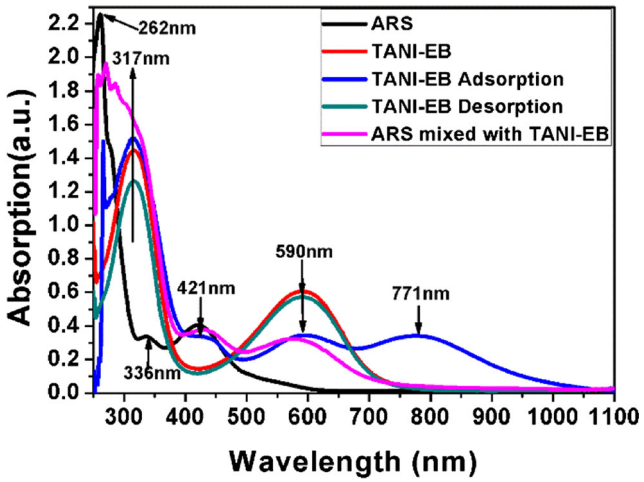

Fig. 8 UV-Vis spectra of the samples (using DMSO as solvent)

between adjacent chains, while the peak at 25.38° is π-π stacking to form well-ordered organic conducting crystals [50]. It is illustrated that there is π-π interaction in addition to the electrostatic effect in the adsorption process.

The FT-IR spectra of pristine TANI-EB, TANI-adsorbed ARS, and TANI-desorbed ARS are shown in Fig. 10 (the important peaks of FT-IR transmittance for different samples and their assignments in Table S4). In the spectra, the main peaks at 1599 and 1510 cm^{-1} are attributed to C=C stretch vibrations of quinoid ring and benzenoid ring in TANI, respectively [51]. The peak at 1296 cm^{-1} is ascribed to the C-N stretching while the peak at 1167 cm^{-1} is ascribed to N-Q-N (Q is quinoid). The peak at 823 cm^{-1} belongs to the out-of-plane bending vibration of –C-H in the benzenoid ring [30, 52]. While in the spectrum of the peak at 1369 cm^{-1} is due to the stretching vibration of the resonance between the C=O group and hydroxyl group in the ARS [53] and the peak at 1032 cm^{-1} corresponds to the stretching vibration of

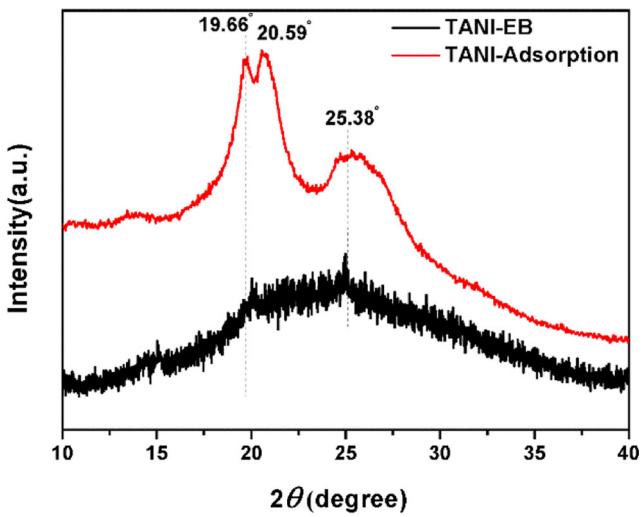

Fig. 9 XRD patterns of TANI-EB and TANI adsorbed ARS

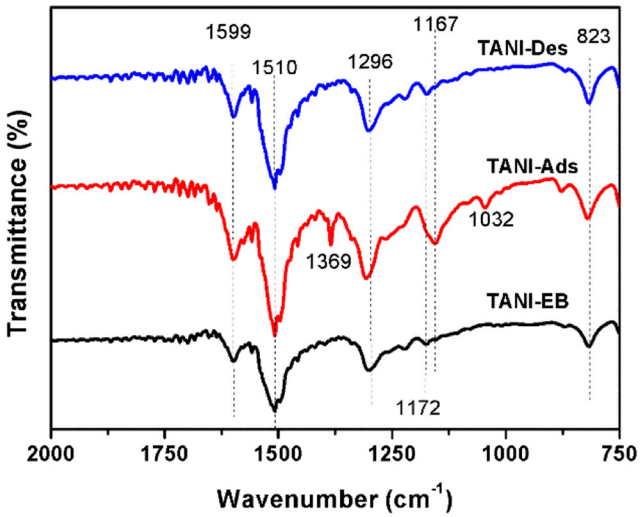

Fig. 10 FT-IR spectra of samples

S=O in $–SO_3^-$ group [54]. These two peaks disappear in the FT-IR spectrum of TANI desorbed, which indicates that the ARS takes off from the TANI. The results of the FT-IR spectra indicate that the ARS can uptake onto the as-prepared TANI-EB and can be almost taken off in the desorption process.

Many reports used doped PANI (in ES phase) as the adsorbent to remove dyes from aqueous solutions, and the plausible adsorption mechanisms were also discussed because some authors found that PANI in emeraldine base (EB) phase cannot remove dyes from aqueous solution [21]. More researchers found that the crystallinity of polyaniline is not significantly affected by the dye adsorption as the structure of PANI is unaltered by the adsorption and desorption of the dye. And the UV-Vis spectrum of polyaniline is also not influenced after the dye adsorbed when the polyaniline in emeraldine salt (ES) phase was employed as adsorbent to remove dye from aqueous solution. Furthermore, the chemical interaction [22] and electrostatic interaction [38] were believed as the main mechanism in the adsorption. However, the specific possible site for the adsorption has never been explanation. Herein, the electrostatic interaction between the positively charged nitrogen atoms in the TANI and the negatively charged $–SO_3^-$ in ARS was testified by UV-Vis and FT-IR spectra. While the π-π interaction for the π-electron-rich molecular structures of TANI-EB and ARS were also proved by XRD pattern and FT-IR spectrum. The explicit adsorption mechanism can be proved expressly for the relatively clearer molecular structure of TANI than that of PANI. It further illustrates that the adsorption mechanism of dye onto PANI can be better understood by using TANI as the model compound of PANI. Furthermore, this study also found TANI in EB phase is possible to be as a potential adsorbent to remove dye from aqueous solution, which is different from the reports.

Conclusions

In this study, the adsorption performance of the as-prepared TANI-EB for anionic organic dye-ARS was investigated. The positively charged surface of the as-prepared TANI-EB in the pH range of 1–7 was confirmed by zeta potential analysis. And the higher adsorption capacity of TANI-EB for ARS when pH < 7 was consistent with the zeta potential value of the TANI-EB, indicating the electrostatic attraction between TANI-EB and ARS. The Langmuir model was the best fitting isotherm model for the adsorption of ARS onto TANI-EB. The thermodynamic parameters evaluated from the adsorption process confirmed that the adsorption of ARS onto TANI-EB was governed by physisorption process. The as-prepared TANI-EB as the adsorbent can be easily regenerated by acidic and basic solvent operation at least 4 times without obvious loss of the adsorption capacity. The π-π interaction except electrostatic effect between the TANI-EB and ARS was also proved by the FT-IR, UV-Vis, and XRD characterizations. This result illustrates that the adsorption mechanism of organic dye on PANI can be better understood by using TANI as the model compound of PANI for the relatively clearer molecular structure of TANI than that of PANI.

Funding This study was funded by the National Natural Science Foundation of China (grant number 21307098 and 21507104), the Shaanxi Key Research and Development Program, China (grant number 2017SF-386), and the Fundamental Research Funds for the Central Universities of China.

Compliance with ethical standards

Conflict of interest The authors declare that they have no conflict of interest.

References

1. Wang SB, Boyjoo Y, Choueib A, Zhu ZH (2005) Removal of dyes from aqueous solution using fly ash and red mud. Water Res 39: 129–138
2. Gupta VK, Ali I (2008) Removal of endosulfan and methoxychlor from water on carbon slurry. Environ Sci Technol 42:766–770
3. Gupta VK, Gupta B, Rastogi A, Agarwal S, Nayak A (2011) A comparative investigation on adsorption performances of mesoporous activated carbon prepared from waste rubber tire and activated carbon for a hazardous azo dye-acid blue 113. J Hazard Mater 186:891–901
4. Jabbari V, Veleta JM, Zarei-Chaleshtori M, Gardea-Torresdey J, Villagrán D (2016) Green synthesis of magnetic MOF@GO and MOF@CNT hybrid nanocomposites with high adsorption capacity towards organic pollutants. Chem Eng J 304:774–783
5. Zhang CF, Qiu LG, Ke F et al (2013) A novel magnetic recyclable photocatalyst based on a core-shell metal-organic framework Fe3O4@MIL-100(Fe) for the decolorization of methylene blue dye. J Mater Chem A 1:14329–14334
6. Yao Y, Xu F, Chen M, Xu Z, Zhu Z (2010) Adsorption behavior of methylene blue on carbon nanotubes. Bioresour Technol 101: 3040–3046
7. Li JR, Kuppler RJ, Zhou HC (2009) Selective gas adsorption and separation in metal-organic frameworks. Chem Soc Rev 38:1477–1504
8. Shen Y, Fang QL, Chen BL (2015) Environmental applications of three-dimensional graphene-based macrostructures: adsorption, transformation, and detection. Environ Sci Technol 49:67–84
9. Cao J, Zhu Y, Bao K, Shi L, Liu S, Qian Y (2009) Microscale Mn2O3 hollow structures: sphere, cube, ellipsoid, dumbbell, and their phenol adsorption properties. J Phys Chem C 113: 17755–17760
10. Zhang ZY, Xiao F, Guo YL, Wang S, Liu Y (2013) One-pot self-assembled three-dimensional TiO2-graphene hydrogel with improved adsorption capacities and photocatalytic and electrochemical activities. ACS Appl Mater Interfaces 5:2227–2233
11. Li JJ, Feng JT, Yan W (2013) Excellent adsorption and desorption characteristics of polypyrrole/TiO2 composite for methylene blue. Appl Surf Sci 279:400–408
12. Jiangtao F, Jingjing L, Wei L et al (2014) Synthesis of polypyrrole nano-fibers with hierarchical structure and its adsorption property of acid red G from aqueous solution. Synth Met 191:66–73
13. Ayad MM, Abu El-Nasr A (2010) Adsorption of cationic dye (methylene blue) from water using Polyaniline Nanotubes Base. J Phys Chem C 114:14377–14383
14. Bhadra S, Khastgir D, Singha NK, Lee JH (2009) Progress in preparation, processing and applications of polyaniline. Prog Polym Sci 34:783–810
15. Li D, Huang JX, Kaner RB (2009) Polyaniline nanofibers: a unique polymer nanostructure for versatile applications. Acc Chem Res 42: 135–145
16. Huang J, Virji S, Weiller BH, Kaner RB (2004) Nanostructured polyaniline sensors. Chem-Eur J 10:1314–1319
17. Cong HP, Ren XC, Wang P, Yu SH (2013) Flexible graphene-polyaniline composite paper for high-performance supercapacitor. Energy Environ Sci 6:1185–1191
18. Xu JJ, Wang K, Zu SZ, Han BH, Wei Z (2010) Hierarchical nanocomposites of polyaniline nanowire arrays on graphene oxide sheets with synergistic effect for energy storage. ACS Nano 4: 5019–5026
19. Ayad M, El-Hefnawy G, Zaghlol S (2013) Facile synthesis of polyaniline nanoparticles; its adsorption behavior. Chem Eng J 217:460–465
20. Guo X, Fei GT, Su H, Zhang LD (2011) Synthesis of polyaniline micro/nanospheres by a copper(II)-catalyzed self-assembly method with superior adsorption capacity of organic dye from aqueous solution. J Mater Chem 21:8618–8625
21. Mahanta D, Madras G, Radhakrishnan S, Patil S (2009) Adsorption and desorption kinetics of anionic dyes on doped polyaniline. J Phys Chem B 113:2293–2299
22. Mahanta D, Madras G, Radhakrishnan S, Patil S (2008) Adsorption of sulfonated dyes by polyaniline emeraldine salt and its kinetics. J Phys Chem B 112:10153–10157
23. Zhou QX, Wang YQ, Xiao JP, Fan H (2016) Adsorption and removal of bisphenol A, alpha-naphthol and beta-naphthol from aqueous solution by Fe3O4@polyaniline core-shell nanomaterials. Synth Met 212:113–122
24. Sun YB, Shao DD, Chen CL, Yang S, Wang X (2013) Highly efficient enrichment of radionuclides on graphene oxide-supported polyaniline. Environ Sci Technol 47:9904–9910
25. Huang J, Kaner RB (2003) A general chemical route to polyaniline nanofibers. J Am Chem Soc 126:851–855
26. Wang Y, Tran HD, Liao L, Duan X, Kaner RB (2010) Nanoscale morphology, dimensional control, and electrical properties of oligoanilines. J Am Chem Soc 132:10365–10373

27. Wang Y, Liu J, Tran HD, Mecklenburg M, Guan XN, Stieg AZ, Regan BC, Martin DC, Kaner RB (2012) Morphological and dimensional control via hierarchical assembly of doped oligoaniline single crystals. J Am Chem Soc 134:9251–9262
28. Bell OA, Wu G, Haataja JS, Brömmel F, Fey N, Seddon AM, Harniman RL, Richardson RM, Ikkala O, Zhang X, Faul CFJ (2015) Self-assembly of a functional oligo(aniline)-based amphiphile into helical conductive nanowires. J Am Chem Soc 137: 14288–14294
29. Thomas JO, Andrade HD, Mills BM, Fox NA, Hoerber HJK, Faul CFJ (2015) Imaging the predicted isomerism of oligo(aniline)s: a scanning tunneling microscopy study. Small 11:3430–3434
30. Lv W, Feng JT, Yan W, Faul CFJ (2014) Self-assembly and pH response of electroactive liquid core-tetra(aniline) shell microcapsules. J Mater Chem B 2:4720–4725
31. Yu JC, Yu JG, Ho WK, Zhang L (2001) Preparation of highly photocatalytic active nano-sized TiO2 particles via ultrasonic irradiation. Chem Commun 19:1942–1943
32. Feng JT, Zhu JW, Lv W, Li J, Yan W (2015) Effect of hydroxyl group of carboxylic acids on the adsorption of acid red G and methylene blue on TiO2. Chem Eng J 269:316–322
33. Moreno-Castilla C (2004) Adsorption of organic molecules from aqueous solutions on carbon materials. Carbon 42:83–94
34. Yagub MT, Sen TK, Afroze S, Ang HM (2014) Dye and its removal from aqueous solution by adsorption: a review. Adv Colloid Interf Sci 209:172–184
35. Salleh MAM, Mahmoud DK, Karim W et al (2011) Cationic and anionic dye adsorption by agricultural solid wastes: a comprehensive review. Desalination 280:1–13
36. Zhang X, Bai RB (2002) Adsorption behavior of humic acid onto polypyrrole-coated nylon 6,6 granules. J Mater Chem 12: 2733–2739
37. Srinivasan A, Viraraghavan T (2010) Decolorization of dye wastewaters by biosorbents: a review. J Environ Manag 91:1915–1929
38. Patra BN, Majhi D (2015) Removal of anionic dyes from water by potash alum doped polyaniline: investigation of kinetics and thermodynamic parameters of adsorption. J Phys Chem B 119:8154–8164
39. Ai LH, Li M, Li L (2011) Adsorption of methylene blue from aqueous solution with activated carbon/cobalt ferrite/alginate composite beads: kinetics, isotherms, and thermodynamics. J Chem Eng Data 56:3475–3483
40. Liu TH, Li YH, Du QJ et al (2012) Adsorption of methylene blue from aqueous solution by graphene. Colloids Surf B 90:197–203
41. Fernandes AN, Almeida CAP, Debacher NA, Sierra MMS (2010) Isotherm and thermodynamic data of adsorption of methylene blue from aqueous solution onto peat. J Mol Struct 982:62–65
42. Kim H, Park JW (2010) Self-assembly of rod-coils consisting of tetraaniline and alkyl chains in different oxidation states. J Mater Chem 20:1186–1191
43. Shao ZC, Yu Z, Hu JC, Chandrasekaran S, Lindsay DM, Wei Z, Faul CFJ (2012) Block-like electroactive oligo(aniline)s: anisotropic structures with anisotropic function. J Mater Chem 22:16230–16234
44. Panizza M, Oturan MA (2011) Degradation of alizarin red by electro-Fenton process using a graphite-felt cathode. Electrochim Acta 56:7084–7087
45. Wu KB, Hu SS (2004) Deposition of a thin film of carbon nanotubes onto a glassy carbon electrode by electropolymerization. Carbon 42:3237–3242
46. Wei ZX, Laitinen T, Smarsly B, Ikkala O, Faul CFJ (2005) Self-assembly and electrical conductivity transitions in conjugated oligoaniline - surfactant complexes. Angew Chem Int Ed 44:751–756
47. Yan Y, Wang R, Qiu XH, Wei Z (2010) Hexagonal superlattice of chiral conducting polymers self-assembled by mimicking beta-sheet proteins with anisotropic electrical transport. J Am Chem Soc 132:12006–12012
48. Li XY, Pignatello JJ, Wang YQ, Xing B (2013) New insight into adsorption mechanism of ionizable compounds on carbon nanotubes. Environ Sci Technol 47:8334–8341
49. Lin DH, Xing BS (2008) Tannic acid adsorption and its role for stabilizing carbon nanotube suspensions. Environ Sci Technol 42: 5917–5923
50. Wang Y, Liu JL, Tran HD, Mecklenburg M, Guan XN, Stieg AZ, Regan BC, Martin DC, Kaner RB (2012) Morphological and dimensional control via hierarchical assembly of doped oligoaniline single crystals. J Am Chem Soc 134:9251–9262
51. Yang ZF, Wang XT, Yang YK, Liao Y, Wei Y, Xie X (2010) Synthesis of electroactive tetraaniline-PEO-tetraaniline triblock copolymer and its self-assembled vesicle with acidity response. Langmuir 26:9386–9392
52. Simotwo SK, DelRe C, Kalra V (2016) Supercapacitor electrodes based on high-purity electrospun polyaniline and polyaniline-carbon nanotube nanofibers. ACS Appl Mater Interfaces 8: 21261–21269
53. Wu LM, Forsling W, Holmgren A (2000) Surface complexation of calcium minerals in aqueous solution 4. The complexation of alizarin red S at fluorite-water interfaces. J Colloid Interface Sci 224: 211–218
54. Pielesz A, Wkochowicz A, Binias W (2000) The evaluation of structural changes in wool fibre keratin treated with azo dyes by Fourier transform infrared spectroscopy. Spectrochim Acta A 56: 1409–1420